ADVANCED ENERGY MATERIALS
www.advenergymat.de

Seasonal Effects on Outdoor Stability of Perovskite Solar Cells

*Ritesh Kant Gupta, D. Kishore Kumar, Vediappan Sudhakar, Johannes M. Beckedahl, Antonio Abate, Eugene A. Katz, and Iris Visoly-Fisher**

The critical challenge for the commercialization of perovskite solar cells (PSCs) is their operational stability. PSCs' outdoor operation exposes the cells to a combination of stress factors that are difficult to reproduce by indoor testing due to diurnal and seasonal variations. This highlights the need for outdoor testing under operational conditions. The effect of climate conditions on outdoor operational *lifetime/ degradation* of n-i-p PSCs is systematically studied herein. Their lifetime indicators are determined in different seasons, and correlated with the outdoor irradiance and temperatures measured simultaneously. Based on this outdoor measurement analysis and indoor light cycling stability tests, it is suggested that ambient temperatures induce a more significant effect than the irradiance on the PSC's *lifetime/ degradation*. The study also suggests different roles played by the temperatures during the diurnal light versus dark periods: the day/ light time maximum temperatures have a more significant effect on the long-term degradation. In contrast, minimum temperatures during the night/ dark cycles significantly affected the diurnal reversible degradation and the initial fast degradation. The results show that the commonly used lifetime indicators T80 and T50 are climate-dependent, and their use for comparative purposes is valid only if measured in similar climatic conditions.

1. Introduction

The performance of perovskite solar cells (PSCs) has recently reached certified power conversion efficiency (PCE) of 26.7%.[1] However, the critical challenge for PSC commercialization is their operational stability, limited by the PSCs' vulnerability to multiple stress and environmental factors.[2,3] PSCs outdoor operation exposes the cells to a combination of stress factors that are difficult to reproduce by indoor testing due to diurnal and seasonal variations. This highlights the need for outdoor testing under operational conditions, including maximum power point tracking (MPPT) and device encapsulation for protection from humidity- and oxygen- induced degradation.[4,5] Published data from such testing currently needs to be improved, possibly due to its time-consuming nature and the complex experimental requirements.[3] Most outdoor tests of single junction devices were applied to p-i-n[6–13] or carbon-based PSCs,[14–17] with few studies of larger scale devices: p-i-n[18] or carbon-based[19] modules and n-i-p panels.[20]

Operational conditions outdoors include diurnal light/ dark cycling, with varying cell temperature and sunlight intensity and spectrum. PSC stability and lifetime are determined by day/ night transient performance variations, superimposed on non-reversible, long-term degradation processes.[21–23] Various dynamics were demonstrated for PSC performance during light/ dark cycles. PSCs showing degradation under illumination may recover during night-time, and the loss in PSC performance under light exposure can be fully or partially compensated.[24–26] The opposite behavior was also observed in PSCs: PCE degradation during dark periods and its recovery under subsequent illumination.[22,27] Furthermore, these two opposite trends were observed for the same devices at various degradation states.[22]

Reversible degradation mechanisms are thought to include light-induced formation of bulk nonradiative recombination defects and their annihilation,[18,28,29] ion migration in either direction, where halide and cation vacancies migrate at different timescales,[25,30] and reversible perovskite decomposition (self-healing) by defect healing and bond recovery.[31–33] Reversible PCE improvement under illumination, i.e., the

R. K. Gupta, D. K. Kumar, V. Sudhakar, E. A. Katz, I. Visoly-Fisher
Ben-Gurion Solar Energy Center
Swiss Inst. for Dryland Environmental and Energy Research
Jacob Blaustein Institutes for Desert Research
Ben-Gurion University of the Negev
Midreshet Ben-Gurion 8499000, Israel
E-mail: irisvf@bgu.ac.il
J. M. Beckedahl, A. Abate
HySPRINT Photovoltaics Lab
Department of Active Materials and Interfaces for Perovskite Solar Cells (SE-AMIP)
Helmholtz-Zentrum für Materialien und Energie
12489 Berlin, Germany

The ORCID identification number(s) for the author(s) of this article can be found under https://doi.org/10.1002/aenm.202403844

DOI: 10.1002/aenm.202403844

well-known light soaking effect, was mainly attributed to trap filling upon illumination.[34] The "day–night" metastability of PSCs raises the need for stability testing under light cycling,[6] and further under outdoor conditions that add variability in irradiance and temperature during the cycles.[26,35] Accordingly, standard light cycling (LC) and outdoor stability test protocols were recently proposed as part of a consensus statement for PSC stability testing.[5]

The effect of climate conditions on the *photovoltaic performance* of PSCs showed, for example, increased daily efficiency (performance factor) of p-i-n PSCs in the summer compared to colder seasons, presumably due to a blueshift in the solar spectrum during the summer.[6] However, printed p-i-n perovskite-based devices measured in the same location showed decreased performance during the summer months.[7] Jost et al. analyzed PSC performance dependence on the incident solar irradiance and air temperature and observed a weak effect of diurnal variations in solar irradiance on the photovoltage hence the output power followed the maximum current density variations.[9,11] A weak temperature dependence of the PSCs' PCE was demonstrated.[20,26]

Long-term PSC *lifetime/ degradation* variations, rather than immediate *photovoltaic performance* variations, may also be attributed to varying climate conditions. PSC lifetime is frequently quantified by T80, the time to reach 80% of the initial PCE. A broad range of lifetimes of encapsulated single-junction perovskite-based cells and modules at outdoor operation at MPP were reported, ranging from time scales of years[6–8] to months, weeks or days.[9–16,18–20] Such variability may be attributed to different cell architectures and the climate conditions in the different locations and seasons at which the outdoor exposure took place. Specifically, seasonal stability dependence has been previously detected in p-i-n PSCs measured in the same location, with slower long-term degradation during winter than during summer, resulting in shorter T80 values for PSC whose exposure started during the summer.[6,9] A suggested explanation to these seasonal effects was that irradiation and temperature profiles on a given day prevent the achievement of complete recovery of the reversible degradation, leading to accumulated degradation.[6,22] It was also suggested that slower initial degradation, sometimes termed "burn-in", occurred in p-i-n PSCs during the colder, less sunny months, yielding longer T80 values.[9] On the other hand, similar stabilities of identical carbon-based PSCs were measured in both Spain and Malta, although the irradiance conditions were very different: 2-axis solar tracking (higher irradiance) and UV filtering were used in Spain, while a fixed platform with no filtering was used in Malta.[17] Jiang et al. modelled outdoor ageing behavior using temperature-dependent degradation rates from indoor stability tests under constant illumination, suggesting that temperature is a significant factor in determining outdoor stability.[12] These sporadic data indicate a seasonal effect on T80, and call for a systematic study to assess the specific outdoor climate parameters responsible for this effect.

Herein we systematically study the effect of climate conditions on outdoor operational *lifetime/ degradation* of n-i-p PSCs, a type of PSCs less frequently studied under outdoor testing, despite its advantages for up-scaling.[20] We note that although several similarities were found to stability characteristics of p-i-n cells (see below), the relevance of the results and conclusions drawn herein to other cell architectures should be verified. We determine the n-i-p devices' lifetime indicators as T80 and T50 (the time until PCE drops to 50% of its initial value) in different seasons and correlate them with the outdoor irradiance and temperatures measured simultaneously. Based on this outdoor measurement analysis and indoor LC stability tests, we suggest that ambient temperatures induce a more significant effect than the irradiance on the PSC's *lifetime/ degradation*. We also suggest different roles played by the temperatures during the diurnal light versus dark periods: the day/ light time maximum temperatures have a more significant effect on the long-term degradation. In contrast, minimum temperatures during the night/ dark cycles significantly affected the diurnal reversible degradation and the initial fast PCE degradation. Our results show that T80 and T50 are climate dependent, and using only these metrics may be unsuitable for comparison of PSC stability when measured outdoors at different locations and/ or climates.

Determining the climate-dependent performance dynamics is significant for using PSCs in tandem devices with Si solar cells, where continuously matching their electrical outputs is critical.[36] It is also important for predicting the long-term energy output of PSCs, especially when reversible processes are activated by the changing climate factors and can reverse, at least in part, short-term degradation losses.[37] As temperature-related photoinduced dynamics are commonly related to ion migration (see below), our findings can also be relevant for other perovskite-based optoelectronic devices such as light-emitting diodes,[38] as well as memristors based on ionic effects triggered by optical inputs.[39]

2. Results and Discussion

In this work, n-i-p PSCs of architecture FTO/ c-TiO_2/ m-TiO_2/ triple cation, mixed halide perovskite/ spiro-MeOTAD/ Au have been fabricated and studied (see Experimental details). The initial photovoltaic performance parameters are presented in the Supporting Information (Table S1 and Figure S1). Encapsulated PSCs were mounted outdoors on a dual-axis solar tracker in Sede Boqer, Israel at different dates between August 2022 and December 2023 and kept at MPP conditions, while the ambient temperatures and irradiance were simultaneously recorded on the same tracker. PCE values were calculated from the ratio between the maximum power output of the PSC and the simultaneously measured solar irradiance.

The T80 values of 36 devices measured outdoors are presented in **Figure 1a**, showing large variations from a few tens of hours to hundreds of hours. To understand these variations, we separated the T80 values according to the season of measurement, as shown in Figure 1b. Significant differences were observed between T80 values in summer-fall and those measured in winter-spring, with more minor variations in each season. Shorter T80 values of our n-i-p PSCs during the warmer seasons agree well with such findings in p-i-n PSCs.[6,9] Seasonal T50 values show the same trend, though with smaller variations between summer-fall and winter-spring, where the average values fall within the range of other seasons, suggesting that the seasonal effect is more significant in short(er) term degradation.

Typical PCE variations with time for outdoor measurements during different seasons are presented in **Figure 2**. The PCE variations mostly follow maximum power point current (I_{mpp})

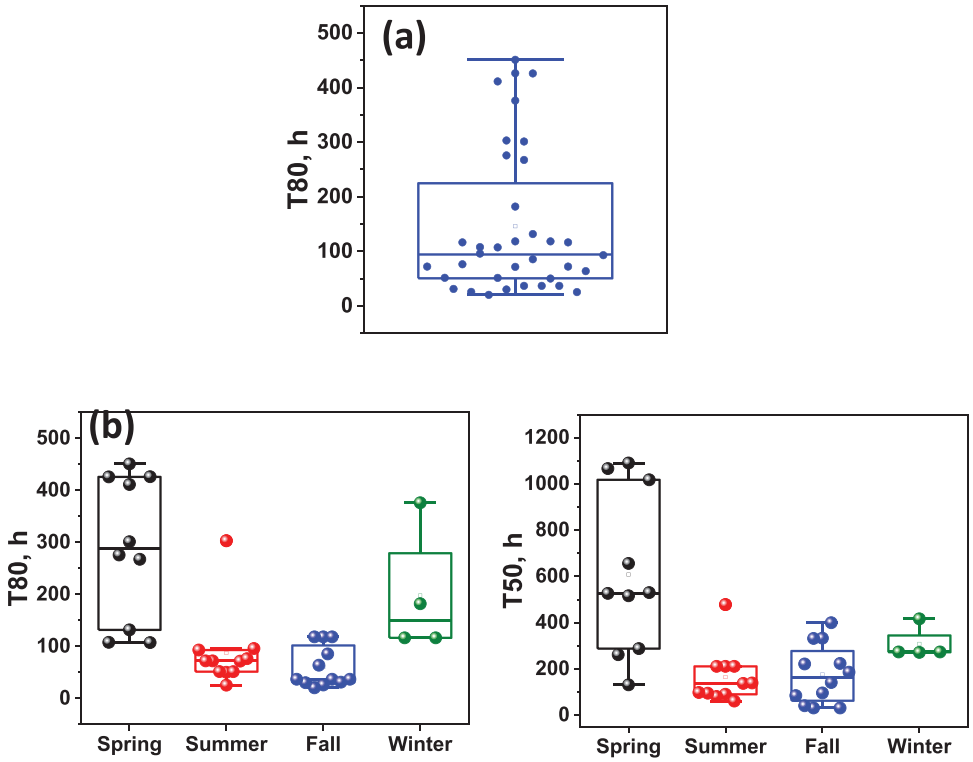

Figure 1. a) T80 values of all PSCs tested outdoors, b) T80 (left panel) and T50 (right panel) values of the outdoor measured PSCs in different seasons.

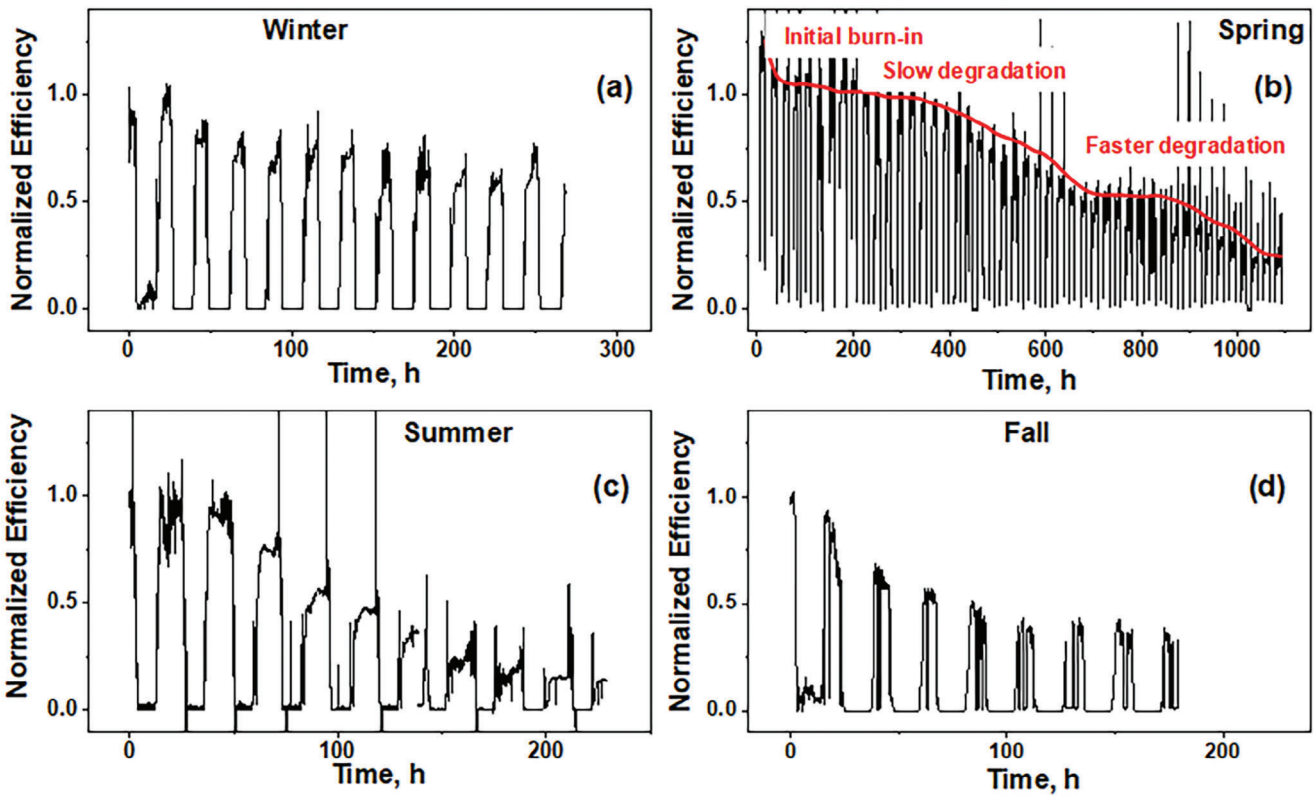

Figure 2. Representative outdoor (normalized) PCE variations with time for PSC measured outdoors in Sede Boqer during a) winter, b) spring, c) summer, d) fall. The line in panel b is presented as a guide to the eye to indicate the different degradation stages.

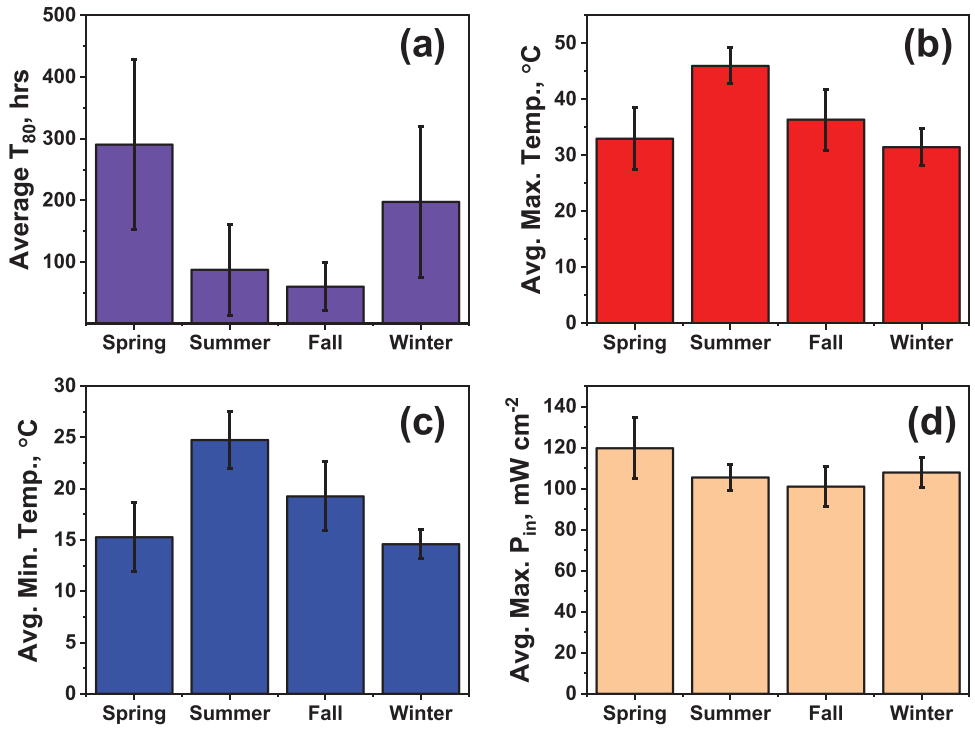

Figure 3. Average seasonal values and standard deviations for a) Estimated outdoor T80, b) Daily maximum temperature, c) Daily minimum temperature, and d) Daily maximum solar irradiance.

variations, while the maximum power point voltage (V_{mpp}) is found to be much more stable (Figure S2a–d, Supporting Information). The n-i-p PSCs used herein always showed PCE degradation during the night. In most cases, PCE improved during the day, however this behavior was season dependent. PSC degradation in the dark was previously observed in various PSC architectures,[6,22,24,27,40,41] and was attributed to ion migration.[27,40–42] This reversible "fatigue" behavior was found to be temperature-dependent and to correlate with increased capacitance during the light period, decreasing in the dark.[27] Such dynamics were reduced by an interfacial treatment acting as a migration barrier and enhancing iodide defect healing in the perovskite, pointing to iodide as the migrating species.[40] Reversible photoinduced phase segregation is unlikely to explain such dynamics in our PSCs, due to the small Br content and the triple cation composition, that was found to have improved structural stability.[43,44] While it is outside of the scope of this paper, we believe that the mechanism responsible for it deserves further studies. Such research is in progress in our laboratory and will be addressed in a separate publication.

PCE variations show three stages characterized by different long-term degradation rates and changes in day-night dynamics, as demonstrated in Figure 2b: i) initial fast PCE degradation, "burn-in", characterized by PCE degradation during both day and night. To the best of our knowledge, outdoor PSC metastability including degradation during both day and night has not been described in the literature yet; ii) a slower long-term degradation stage, characterized by fast PCE increase during the morning ("light soaking") followed by mostly stable PCE for the rest of the day; and iii) faster long-term degradation, along with slow increase of the PCE during the daytime.

The temporal PCE variations in spring show a short (i) "burn in" stage followed by a relatively long (ii) slower degradation stage (Figure 2b). The temporal PCE variations during the winter show only stage (ii) (Figure 2a). As stage (ii) sets slower long-term degradation, this may explain the longer T80 values determined during these seasons. PCE temporal tracks measured during the summer show a transition from a short stage (i) to stage (iii), where the slow PCE increase during the day is sometimes followed by its decrease on the same day (Figure 2c). PCE temporal tracks measured in the fall are characterized by long (i) "burn in" periods with PCE degradation during the day and during the night (Figure 2d). As stages (i) and (iii) include faster long-term PCE degradation rates, this behavior correlated well with the shorter T80 and T50 values measured in these seasons (Figure 1). The seasons with shorter lifetimes, summer and fall, are characterized by short or no stage (ii), while winter and spring, showing longer lifetimes, result in long (ii) stages. Another difference is in the (i) burn-in stage, which is significantly shorter in winter and spring compared to summer and fall. We postulate that these differences result from the different characteristic temperatures in these seasons (see below).

To better understand the seasonal parameters' effect on T80, the outdoor seasonal T80 values were compared with the seasonal variations in ambient temperatures and solar irradiance during exposure (**Figure 3**; Figures S3–S5, Supporting Information). It is noted that the device temperature is expected to be higher than the ambient temperature. Modeling suggested a

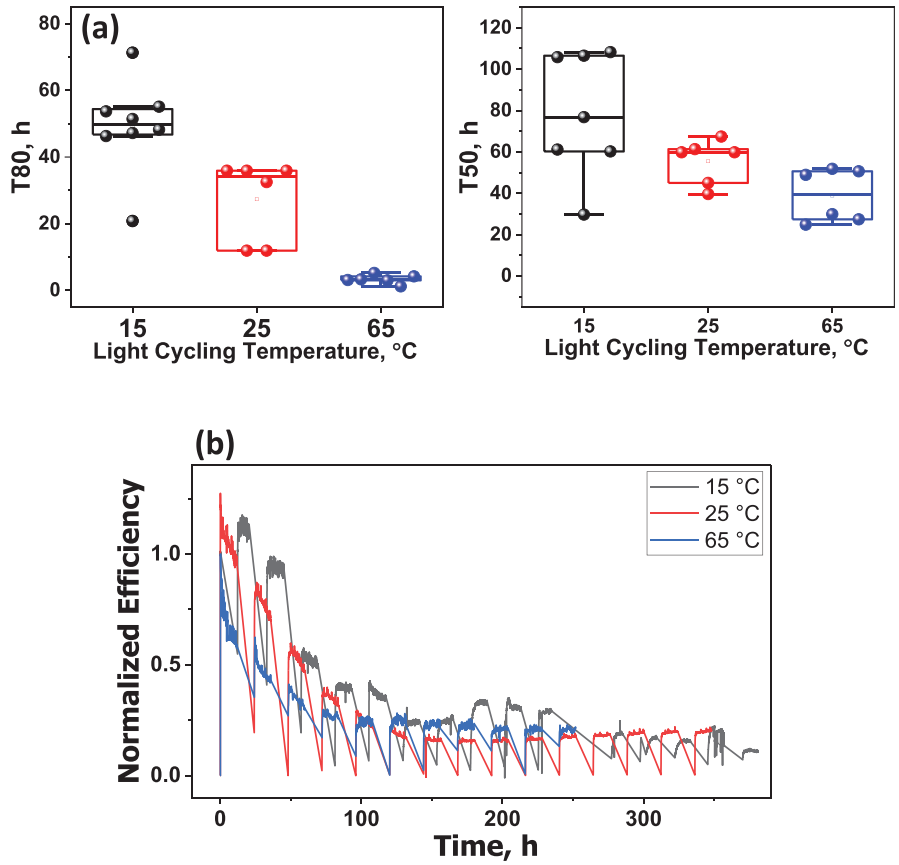

Figure 4. a) T80 (left panel) and T50 (right panel) values from indoor light cycling experiments at different temperatures. b) PCE versus time tracks, each averaged from measuring 6 PSCs, from indoor light cycling experiments at different temperatures. The related J_{mpp} and V_{mpp} versus time tracks are shown in Figure S6 (Supporting Information).

temperature increase of 20–29 °C in the Negev desert under one sun irradiance,[9,45] while empirical estimates suggested higher temperatures.[12] It can be seen that higher average daily maximum and minimum ambient temperatures (Figure 3b,c) are correlated with lower average T80 values during fall and summer (Figure 3a). At the same time, no correlation was found between the variations in average T80 and the daily temperature gradients (Figure S4, Supporting Information). The dominance of the temperatures in outdoor long-term degradation was also previously demonstrated for p-i-n cells.[12]

T80 was previously reported to decrease with increasing light intensity in indoor stressing under continuous illumination.[12,46] However, in our outdoor study, a relatively weak correlation is observed between average daily maximum irradiance and average T80 values (Figure 3a,d). It is noted that the variations in maximum irradiance between the seasons are minor and within error, possibly due to our geographical location and the use of a dual-axis solar tracker. Specifically, the average maximum daily irradiance in the winter and summer seasons are somewhat similar, while the T80 values in these seasons are very different. No correlation was found between T80 value variations and the average integrated daily irradiance (Figure S5, Supporting Information), within the ca. 20% variations of the integrated irradiance between seasons.

Indoor light cycling (LC) stability tests, with illumination by a solar simulator, were used to disentangle the effects of temperature from that of irradiance. The tests were performed at 12 h:12 h light/ dark cycles, under simulated one sun irradiance, at varying temperatures, based on the ISOS-LC-2 protocol.[5] The results are presented in **Figure 4**. In accord with the outdoor results, T80 and T50 values from indoor light cycling experiments decrease with increasing temperature (Figure 4a). Both T80 and T50 values from LC testing are smaller than the corresponding metrics determined outdoors (Figure 3a). Degradation acceleration is attributed to larger integrated irradiance during the light cycle (ca. 1200 mW•hr/cm^2) compared to those estimated for our outdoor conditions (600–800 mW•hr/cm^2, Figure S3, Supporting Information), combined with similar temperatures during light- and dark- cycles (see below).

We have used the T80 data from LC tests at different (constant) temperatures to estimate the activation energy for degradation based on the Arrhenius relation and found an apparent activation energy of 0.45 eV (Figure S4, Supporting Information). This value is within the range previously found for interfacial ion migration (0.24–0.59 eV depending on the device components[12,46]), although these values were calculated from testing p-i-n architecture rather than n-i-p, under constant illumination rather than LC. This may indicate that degradation under constant

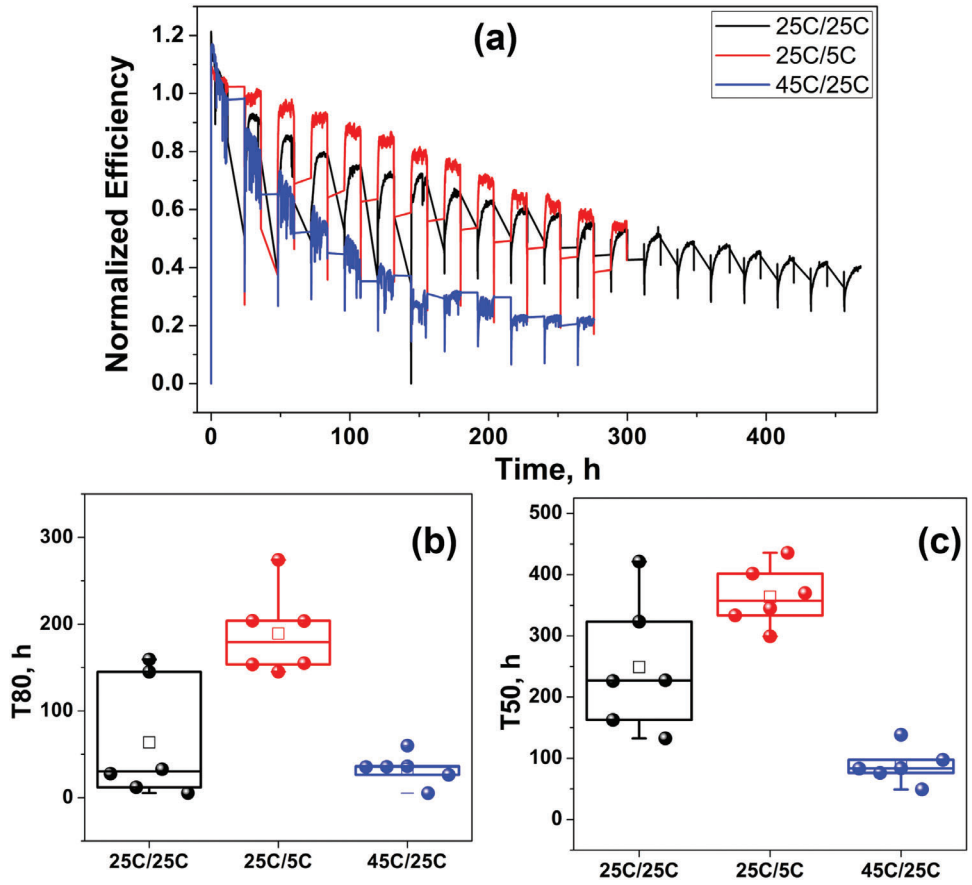

Figure 5. a) Normalized PCE versus time tracks from indoor light cycling experiments at temperatures varying between dark and light periods, as indicated in the legend. Each track represents the average of such tracks of six PSC devices. The related J_{mpp} and V_{mpp} versus time tracks are shown in Figure S7 (Supporting Information). b) T80 and c) T50 values from indoor light cycling experiments at temperatures varying between dark and light periods. The slight discrepancy between T80 values at 25C/25C and at 25C in Figure 4 might be attributed to the different illumination spectrum used in these measurements (see Experimental Section).

temperatures and LC follows similar degradation mechanisms operative under constant illumination, further demonstrating the relative significance of the temperature for photodegradation. We note that the dominant degradation mechanism in our n-i-p PSCs is out of the scope of this research and will be presented in a separate contribution.

The temporal PCE tracks at 25 and 65 °C (Figure 4b) show extended (4–6 cycles) (i) "burn in" periods with PCE degradation during the day and during the night, resembling accelerated fall outdoor behavior (Figure 2d). The temporal PCE track at 15 °C (Figure 4b) shows largely similar long-term degradation but little, if any, degradation during the light cycle, closer to springtime outdoor trend shown in Figure 2b. This correlates well with the concluded temperature variations that induce seasonal effects. The effect of the temperature is also noted on the overall degradation rate during "burn-in", resulting in more significant differences between T80 values compared to those for T50.

We have further modified the LC tests to include different temperatures during light and dark periods. The dark period temperature was kept equal to or lower than that of the light period, qualitatively correlated with the temperature regime at outdoor testing. The test temperatures were: 25C/25C – 25 °C at both dark and light periods, 25C/5C – 25 °C during light periods, 5 °C during dark periods, 45C/25C – 45 °C during light periods, 25 °C during dark periods. The results are presented in **Figure 5**.

We find that a lower temperature (5 °C compared to 25 °C) during the dark periods increased T80 to 6–7 cycles, while increased temperatures during the light periods (45 °C compared to 25 °C) did not significantly affect the average T80, reaching T80 within 2–3 cycles. Careful examination of the temporal PCE tracks in Figure 5a shows that reduced temperatures in the dark decreased the dark-period degradation, resulting in lower degradation rates at the initial stages thus significantly affecting T80. On the other hand, the long-term degradation trends of PSCs measured in 25C/25C or 25C/5C overlapped at a longer time of >200 hr, resulting in similar long-term degradation despite the different dark period temperatures, indicating that the dark period temperature affects the initial degradation stage but is not significant for long term degradation.

The temperature during the light cycle was found to significantly affect the extent of the (i) "burn in" stage, at which the temporal PCE patterns show PCE degradation during both light and dark cycles: one cycle for 25C/5C and 25C/25C, compared to 6 cycles for 45C/25C (Figure 5a). This effect caused overall

faster long-term degradation for 45C/25C stressed PSCs, as expressed by smaller average T80 and T50 values (Figure 5b,c), suggesting that the "burn in" photodegradation mechanism is temperature-activated. This conclusion aligns with constant temperature LC stability testing showing a strong temperature dependence of PSC stability (Figure 4). These results therefore suggest that day-time maximum temperatures are the climate factor with the most substantial effect on PSC outdoor long-term *lifetime/ degradation*. Temperature-dependent PSC photodegradation was previously attributed to ion migration and accumulation,[12,46,47] causing electric field screening and suppressing charge extraction.[48] J_{sc} losses were found to dominate ion migration-induced degradation,[48,49] in agreement with our finding that PCE variations mostly follow I_{mpp} variations. The mechanism responsible for "burn-in" in encapsulated, fullerene-free PSCs was also previously also associated with defects causing ion redistribution and charge accumulation.[25,50,51] Alternatively, temperature-enhanced "burn-in" due to a J_{sc} drop was attributed to interfacial delamination and micro-cracking due to thermal stress induced by thermal expansion mismatch between the layers.[52]

The effect of a temperature gradient between the dark and light cycles is noted by the PSCs tested at 25C/25C reaching stage (iii) of degradation, characterized by a slow increase of the PCE during the light cycle, faster than those tested at 25C/5C and 45C/25C: the former reached that stage after 6 cycles/ ca. 150 hr while the latter did not reach this stage within 12 cycles/ ca. 300 hr. This points to the interplay between PCE transients during dark and light periods and the overall PSC *lifetime/ degradation*. Previous studies of the effect of thermal cycling during illumination (not associated with light cycling) showed degraded J_{sc} and FF associated with increased series resistance and recombination,[53] however this effect was minimized under forward bias such as V_{MPP} as it was attributed to interfacial ion migration under the varying internal photovoltage.[54] Thermal cycling in the dark was found to induce grain boundary cracking and interfacial delamination due to residual stress and strain.[55] Concurrent thermal and light cycling may cause the combination of these effects, and/ or yield other effects, which we are currently investigating.

The apparent acceleration factors (AFs) of the indoor LC stability tests were calculated with respect to outdoor testing in Sede Boqer in the fall (shortest T80) and the spring (longest T80) seasons and are shown in **Figure 6** and Table S2 (Supporting Information). The AF is the ratio of the degradation rate at the accelerated test to that under operational conditions. The degradation rate can be estimated as 1/T80,[56] hence the AF is the inverse ratio between the estimated T80 values in either test. The temperature acceleration is expected to follow Arrhenius-like relations,[56] as indeed shown by LC tests at constant temperatures (Figure S8, Supporting Information). However, such analysis is unreasonable when the temperatures vary during the test, as occurs outdoors or under LC tests with varying temperatures. A linear dependence of the degradation rate on the integrated irradiance per cycle, as previously assumed for stability testing under inert conditions,[5,57] would yield expected AFs of ca. 1200/(600 to 800) = 1.5 to 2. The apparent AFs are expected to integrate both the irradiance and temperature effects and differ between constant- to cycled- temperatures.

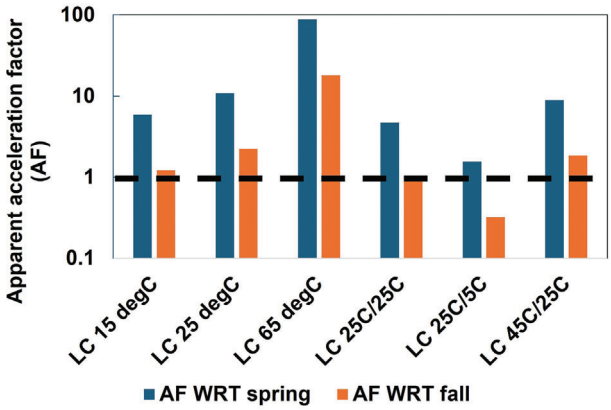

Figure 6. The apparent acceleration factors (AFs) of the indoor LC stability tests with respect to (WRT) outdoor testing in Sede Boqer in the fall and the spring seasons. The dashed line indicates the case of no acceleration (AF = 1). The logarithmic scale was used to highlight both high and low AF values.

It is noted that light cycling at varying temperatures between light and dark periods provides T80 estimates closer to those measured outdoors, while light cycling at constant temperatures yields larger acceleration of the degradation (Figure 6). We postulate that constant temperatures during light and dark cycles enhance dark period degradation in our n-i-p PSCs, which is slowed by lower temperatures at night in outdoor conditions. Hence, indoor light cycling with temperatures during the light cycles close to the maximum daily temperature, and temperatures during the dark cycles close to the minimum daily temperature, might provide a closely related simulation of outdoor PSC *lifetime/ degradation*, even without varying irradiance and temperatures during the cycles.[35] Indeed, 45C/25C provides conditions close to those noted in the fall temperature-wise (Figure 3), and an AF ≅ 1. The significance of the dark period temperature in determining T80 is further demonstrated by the indoor LC tests with constant temperatures close to those at night-time in the fall (ca. 20 °C), i.e., 15 °C and 25 °C, yielding values relatively close to AF ≅ 1 for the fall season where the average minimum temperature is ca. 25 °C. However, longer term degradation is expected to be more significantly affected by the temperature at light periods (see above). It should be noted that researchers should verify that the dominant degradation mechanisms are similar in outdoor and indoor such tests.[58]

3. Summary and Conclusion

We have systematically studied the effect of climate conditions on the outdoor operational lifetime of n-i-p PSCs with an architecture of FTO/ c-TiO_2/ m-TiO_2/ triple cation, mixed halide Perovskite/ Spiro-MeOTAD/ Au, that exhibit PCE degradation during dark periods and, to the most part, its recovery under subsequent illumination. We identified three stages of long-term outdoor degradation, including i) initial fast PCE degradation, "burn-in", characterized by PCE degradation during the day and during the night; ii) a slower degradation stage, characterized by fast PCE increase during the morning ("light soaking") followed by mostly stable PCE for the rest of the day; and iii) faster

degradation, characterized by slow increase of the PCE during the daytime. These patterns were found to be characteristic of the studied n-i-p PSCs during outdoor and indoor light cycling (LC) tests. The presence and extent of these stages vary between different seasons and different temperatures during LC. Indoor light cycling with temperatures during the light cycles close to the maximum daily temperature, and temperatures during the dark cycles close to the minimum daily temperature, are suggested to provide closely related simulation of outdoor PSC *lifetime/ degradation*. Empirical acceleration factors are presented and discussed.

We find that the climate parameter mainly affecting PSC *lifetime/degradation* in our geographical location/climate is the ambient temperature, while the seasonal variations in solar irradiance play a more minor role. The temperatures during day/ light cycles affect the extent of the "burn in" stage, at which PCE degrades during both light and dark cycles, by this affecting the lifetime indicators T80 and T50. The temperatures during dark/ night periods were found to control the reversible diurnal degradation processes. Reduced temperatures in the dark decreased the dark-period degradation, resulting in lower degradation rates at the initial stages, but did not strongly affect their long-term degradation. Our results explain why T80 and T50 values are climate-dependent. As T80 and T50 are commonly used as comparative PSC stability indicators, this suggests that such comparison is valid only if measured in similar climatic conditions.

4. Experimental Section

Materials: Formamidinium iodide (FAI, >99.99%), methylammonium bromide (MABr, >99.99%), and TiO_2 Paste – DSL 30NR-D were obtained from Greatcell Solar Materials. Cesium iodode (CsI, >99.0%), lead iodide (PbI2, 99.99%) and lead bromide (PbBr2, >98.0%) were obtained from TCI. Ti-Nanoxide was obtained from Solaronix. Spiro-OMeTAD (99%), tert-butyl pyridine (tBP, 98%), Bis(trifluoromethane)sulfonimide lithium salt (LiTFSi, 99.95%) were obtained from Merck. FK209 Co(III) TFSI salt (FK209, >99%) was obtained from Lumtec. Fluorine-doped tin oxide (FTO) substrates (TEC 7) were purchased from Pilkington. Solvents were dried over molecular sieve: 99.8% dimethylformamide (DMF), 99.8% cholorobenzene, 99.9% Acetonitrile and >99.7% dimethyl sulfoxide (DMSO) were purchased from Thermo Scientific. All materials were used without further purification.

Preparation of Precursor Solutions:

1) For the electron transport layer (ETL), 150 mg of TiO_2 Paste-DSL 30NR-D was dissolved in 1 mL of ethanol and was stirred overnight.
2) For the hole transport layer (HTL), 122 mg of Spiro-OMeTAD in 1 mL of chlorobenzene was prepared. 28.5 µL of tBP, 18 µL of LiTFSi solution (520 mg in 1 mL acetonitrile), and 8 µL of FK209 solution (375 mg in 1 mL acetonitrile) were added to this solution and thoroughly mixed.
3) The perovskite precursor solution was prepared in a N_2 filled glove box following a published protocol.[59] Briefly, 1.5 M PbI2 (691.5 mg) and 1.5 M PbBr2 (110.1 mg) solutions were prepared in a 1 mL and 200 µL mixed solvent (DMF and DMSO ratio 4:1 v/v), respectively, heated at 180 °C for 15 min and cooled down for further use. Simultaneously, 1.5 M CsI stock solution was also prepared in DMSO and heated at 150 °C for 15 min, then cooled down for further use. Thereafter, the PbI2 solution was added to 236.6 mg FAI (1.37 M) to form FAPbI3 precursor solution and PbBr2 solution was added to 30.8 mg MABr (1.37 M) to form MAPbBr3 precursor solution. Both the perovskite precursor solutions were stirred at 70 °C for 15 min. Finally, both FAPbI3 and MAPbBr3 precursor solutions were mixed along with 5 vol% of CsI stock solution to form triple cation perovskite precursor solution of composition $Cs_{0.05}FA_{0.78}MA_{0.17}Pb(I_{0.87}Br_{0.13})_3$. The triple cation perovskite precursor solution was stirred at 70 °C for at least 2 h before coating.

Perovskite Solar Cell (PSC) Fabrication: Prior to the fabrication of PSC, FTOs were sequentially cleaned through sonication in 2% Hellmanex-III solution, deionized water, acetone and isopropanol. Afterward, the substrates were dried and treated under UV-ozone for 30 min. The compact TiO_2 (c-TiO_2) layer was grown on cleaned FTO by spin coating Ti-Nanoxide at 5000 rpm for 30 s, followed by annealing at 550 °C for 1 h in ambient condition and cooled to below 150 °C before further processing. Then the substrates were again UV-ozone treated for 5 min. Thereafter, mesoporous TiO_2 (m-TiO_2) was grown by spin-coating TiO_2 paste solution at 4000 rpm for 10 s. The substrates were then annealed step wise at 125 °C for 5 min, 325 °C for 5 min, 375 °C for 5 min, and finally 450 °C for 30 min in ambient condition and cooled to below 150 °C before further processing. The substrates were then again UV-ozone treated for 5 min. Li doping of TiO_2 layer was then performed by coating LiTFSI solution (10 mg in 1 mL acetonitrile) at 3000 rpm for 10 s and annealing step wise following the protocol for m-TiO_2. The substrates were then again UV-ozone treated for 5 min and transferred to N_2 filled glove box for the deposition of the perovskite and HTL. The triple cation perovskite precursor solution was spin-coated on the FTO/c-TiO_2/m-TiO_2 substrates at a pre-programmed dual step of 400 rpm for 10 s, followed by 4000 rpm for 30 s. Chlorobenzene as an anti-solvent was carefully dripped on the substrate 10 s before the end of the program. Thereafter, the substrates were annealed at 100 °C for 60 min. Spiro-OMeTAD solution was dynamically spin-coated at 4000 rpm for 20 s. Finally, 80 nm thick gold was deposited by thermal evaporation to complete the PSC with architecture FTO/c-TiO_2/m-TiO_2/Perovskite/Spiro/Au. No preconditioning of the solar cells was applied.

Encapsulation of PSCs: Encapsulation was performed in ambient laboratory conditions. The HTL, perovskite, and ETL layers were mechanically removed from the substrate edges. Extended contacts to the top and bottom electrodes were made with copper ribbons using silver paste and allowed to vacuum dry. Then, the devices were protected with Kapton tape to prevent the epoxy from damaging any of the layers. The epoxy and hardener (2,2 bis(4-(2,3epoxypropoxy)phenyl) propane (Nalmat-Trzebinia) were mixed at the ratio of 1:1 v/v and applied on top of the Kapton tape to cover the entire substrate. A 1 mm thick glass slide was then carefully placed on the top to ensure that there were no air bubbles. The substrates are then kept in the dark and allowed to dry overnight. Finally, metal pins were soldered to the copper ribbons for mounting the samples for indoor and outdoor stability studies. We note that such encapsulation differs from the polyisobutylene (PIB)-based encapsulation commonly used in outdoor studies.[60] Further testing of the epoxy-based encapsulation scheme demonstrated that it is ambient resistant with no detectable humidity penetration after ca. 1 month outdoors in an oceanic/ humid continental climate in Berlin in a rainy season (Oct.-Nov. 2023, not shown). Therefore, it has been assumed that seasonal variations in ambient humidity and oxygen do not affect the degradation of the devices studied herein.

PSC Characterization: The initial photovoltaic performance parameters of all cells were measured by current density-voltage (J-V) scans using a Keithley SMU model 2401 under a solar simulator (LCS 100, class ABB, Newport) at the bias range of −0.2–1.2 V and scan rate of ≈140 mV s^{-1}. External quantum efficiency (EQE) spectra were measured using a spectral response measurement system ("TECHNOEXAN" Ltd., Ioffe Physical-Technical Institute, Russia) with monochromated halogen lamp light. Light chopping was applied to use lock-in amplified detection of the signals at a frequency of 75 Hz. The results are presented in Table S1 and Figure S1 (Supporting Information).

MPP Tracking During Photostability Tests: The cells were subjected to indoor light cycling and outdoor tests at MPP conditions using a tracker (MP0205M6, University of Ljubljana, Faculty of Electrical Engineering, Laboratory of Photovoltaics and Optoelectronics), and the maximum current and voltage data was collected at intervals of 30–300 s. The MPPT

algorithm is the commonly used "Perturb and Observe", controlling the gate voltage of the load transistor at time intervals of 0.2 s and voltage steps of 6 mV, resulting in a voltage slew rate of 32 mV s^{-1}. The gate voltage is limited to stay below the open circuit voltage. The raw data files for indoor and outdoor tests (including the measured I_{mpp}, V_{mpp}, ambient irradiance, and temperatures vs time) can be made available upon request from the authors.

Indoor Stability Tests Under a Modified ISOS-LC-2 Protocol: Encapsulated cells were mounted on a temperature-controlled (by water circulation) metal plate set at 15, 25, or 65 °C. 7–9 PSCs were tested in each temperature and exposed to 12 h light, 12 h dark consecutive cycles. The cells were connected to the MPPT. The cells were illuminated during the light cycles by a solar simulator (SolarConstant MHG 4000/2500 solar simulator, K.H. Steuernagel Lichttechnik GmbH) with an intensity of 100 mW cm^{-2}. Light cycling experiments were also carried out at ViperLab facility of HZB in Berlin: 12 h light and 12 h dark cycles were maintained, but three different combinations of temperatures during light and dark cycles were used: i) L25 °C/D25 °C (25 °C during light cycle and 25 °C during dark cycle), ii) L25 °C/D05 °C, and iii) L45 °C/D25 °C. 6 PSCs were tested for each combination. During the light cycles the encapsulated PSCs were illuminated by a metal halide steam lamp (Höhnle) with an intensity of 100 mW cm^{-2}.

Outdoor Stability Tests Under ISOS-O-2 Protocol: At BGU, Sede Boqer, Israel (30.8523° N, 34.7834° E), 36 encapsulated cells, with identical architectures but from various fabrication batches, were connected to the MPPT and mounted on a dual-axis solar tracker, at different start dates within each season. This was done to account for the cell-to-cell variability common to PSCs. The current and voltage data was collected at 30–300 s intervals. The incident solar irradiation and temperature were continuously recorded. Irradiance was recorded with an Eppley Precision Spectral pyranometer and the ambient temperature was monitored using a type-K thermocouple on the solar tracker plate.

Lifetime Indicators: PCE was calculated for each measurement point as P(out)/P(in). The temporal PCE tracks were normalized with respect to the initial PCE values. The seasons were determined in the following date ranges: Summer: June–August of 2022 and 2023; fall: October–November of 2022 and 2023; winter: December 2022 and 2023; spring: February–April of 2023. Both T80 and T50 were estimated once the graph crosses the value of 80% and 50% of the initial PCE value for the last time. In case the last PCE of the previous day was >80% and the first PCE of the next day <80% of the initial PCE, a linear fit was used to estimate the time when PCE crosses the T80 value. In cases where the T80 or T50 were not achieved during a measurement period, the temporal PCE track was extrapolated to estimate these values. The temporal PCE track during light periods (only) was extrapolated linearly/exponentially at times after the initial burn-in stage, as previously suggested for measurements under constant illumination.[56] The results are presented in box plots where the hollow mark is the average value and middle line is the median. The box indicates the range of 25, 75 percentiles, and the limits are 1, 99 percentiles.

Supporting Information

Supporting Information is available from the Wiley Online Library or from the author.

Acknowledgements

This study was supported by the Israel Science Foundation grant #2457/23, the Israel's Ministry of Energy and Infrastructures grant #3-19074/ 222-11-081, and by the European Union through the TESTARE project (grant 101079488). Support and access to infrastructures of Horizon 2020 framework- funded Viperlab- Fully connected virtual and physical perovskite photovoltaics lab, are gratefully acknowledged. R.K.G. is grateful for the Swiss Inst. of Dryland Environmental and Energy Research Postdoctoral fellowship at BGU. D.K.K. is grateful for the Blaustein Postdoctoral fellowship at BGU. V.S. is grateful for the Kreitman Postdoctoral fellowship at BGU.

Conflict of Interest

The authors declare no conflict of interest.

Data Availability Statement

The data that support the findings of this study are available from the corresponding author upon reasonable request.

Keywords

light cycling, outdoors, perovskite solar cells, stability, T80

Received: August 26, 2024
Revised: November 8, 2024
Published online: November 26, 2024

[1] *Best Research-Cell Efficiency Chart*, https://www.nrel.gov/pv/cell-efficiency.html (accessed: August 2024).
[2] D. Zhang, D. Li, Y. Hu, A. Mei, H. Han, *Commun. Mater.* **2022**, *3*, 58.
[3] S.-P. Feng, Y. Cheng, H.-L. Yip, Y. Zhong, P. W. K. Fong, G. Li, A. Ng, C. Chen, L. A. Castriotta, F. Matteocci, L. Vesce, D. Saranin, A. D. Carlo, P. Wang, J. W. Ho, Y. Hou, F. Lin, A. G. Aberle, Z. Song, Y. Yan, X. Chen, Y. Yang, A. A. Syed, I. Ahmad, T. Leung, Y. Wang, J. Lin, A. M. C. Ng, Y. Li, F. Ebadi, et al., *J. Phys.: Mater.* **2023**, *6*, 032501.
[4] M. U. Ali, H. Mo, Y. Li, A. B. Djurišić, *APL Energy* **2023**, *1*, 020903.
[5] M. V. Khenkin, E. A. Katz, A. Abate, G. Bardizza, J. J. Berry, C. Brabec, F. Brunetti, V. Bulović, Q. Burlingame, A. Di Carlo, R. Cheacharoen, Y.-B. Cheng, A. Colsmann, S. Cros, K. Domanski, M. Dusza, C. J. Fell, S. R. Forrest, Y. Galagan, D. Di Girolamo, M. Grätzel, A. Hagfeldt, E. von Hauff, H. Hoppe, J. Kettle, H. Köbler, M. S. Leite, S. Liu, Y.-L. Loo, J. M. Luther, et al., *Nat. Energy* **2020**, *5*, 35.
[6] M. Khenkin, H. Köbler, M. Remec, R. Roy, U. Erdil, J. Li, N. Phung, G. Adwan, G. Paramasivam, Q. Emery, E. Unger, R. Schlatmann, C. Ulbrich, A. Abate, *Energy Environ. Sci.* **2024**, *17*, 602.
[7] J. Li, J. Dagar, O. Shargaieva, O. Maus, M. Remec, Q. Emery, M. Khenkin, C. Ulbrich, F. Akhundova, J. A. Márquez, T. Unold, M. Fenske, C. Schultz, B. Stegemann, A. Al-Ashouri, S. Albrecht, A. T. Esteves, L. Korte, H. Köbler, A. Abate, D. M. Többens, I. Zizak, E. J. W. List-Kratochvil, R. Schlatmann, E. Unger, *Adv. Energy Mater.* **2023**, *13*, 2203898.
[8] Q. Emery, M. Remec, G. Paramasivam, S. Janke, J. Dagar, C. Ulbrich, R. Schlatmann, B. Stannowski, E. Unger, M. Khenkin, *ACS Appl. Mater. Interfaces* **2022**, *14*, 5159.
[9] M. Jošt, B. Lipovšek, B. Glažar, A. Al-Ashouri, K. Brecl, G. Matič, A. Magomedov, V. Getautis, M. Topič, S. Albrecht, *Adv. Energy Mater.* **2020**, *10*, 2000454.
[10] E. Velilla, F. Jaramillo, I. Mora-Seró, *Nat. Energy* **2021**, *6*, 54.
[11] E. Velilla, D. Ramirez, J.-I. Uribe, J. F. Montoya, F. Jaramillo, *Sol. Energy Mater. Sol. Cells* **2019**, *191*, 15.
[12] Q. Jiang, R. Tirawat, R. A. Kerner, E. A. Gaulding, Y. Xian, X. Wang, J. M. Newkirk, Y. Yan, J. J. Berry, K. Zhu, *Nature* **2023**, *623*, 313.
[13] B. Romero, S. Delgado, D. Glowienka, C.-T. Chang, G. d. Pozo, B. Arredondo, D. Martín-Martín, P. Contreras, Y. Galagan, *Sustainable Energy Fuels* **2023**, *7*, 2146.
[14] Z. Fu, M. Xu, Y. Sheng, Z. Yan, J. Meng, C. Tong, D. Li, Z. Wan, Y. Ming, A. Mei, Y. Hu, Y. Rong, H. Han, *Adv. Funct. Mater.* **2019**, *29*, 1809129.
[15] X. Li, M. Tschumi, H. Han, S. S. Babkair, R. A. Alzubaydi, A. A. Ansari, S. S. Habib, M. K. Nazeeruddin, S. M. Zakeeruddin, M. Grätzel, *Energy Technol.* **2015**, *3*, 551.
[16] Y. Reyna, M. Salado, S. Kazim, A. Pérez-Tomas, S. Ahmad, M. Lira-Cantu, *Nano Energy* **2016**, *30*, 570.

[17] F. De Rossi, J. Barbé, D. M. Tanenbaum, L. Cinà, L. A. Castriotta, V. Stoichkov, Z. Wei, W. C. Tsoi, J. Kettle, A. Sadula, J. Chircop, B. Azzopardi, H. Xie, A. Di Carlo, M. Lira-Cantú, E. A. Katz, T. M. Watson, F. Brunetti, *Energy Technol.* **2020**, *8*, 2000134.
[18] V. Stoichkov, N. Bristow, J. Troughton, F. De Rossi, T. M. Watson, J. Kettle, *Sol. Energy* **2018**, *170*, 549.
[19] Y. Hu, S. Si, A. Mei, Y. Rong, H. Liu, X. Li, H. Han, *Sol. RRL* **2017**, *1*, 1600019.
[20] S. Pescetelli, A. Agresti, G. Viskadouros, S. Razza, K. Rogdakis, I. Kalogerakis, E. Spiliarotis, E. Leonardi, P. Mariani, L. Sorbello, M. Pierro, C. Cornaro, S. Bellani, L. Najafi, B. Martín-García, A. E. Del Rio Castillo, R. Oropesa-Nuñez, M. Prato, S. Maranghi, M. L. Parisi, A. Sinicropi, R. Basosi, F. Bonaccorso, E. Kymakis, A. Di Carlo, *Nat. Energy* **2022**, *7*, 597.
[21] K. Domanski, E. A. Alharbi, A. Hagfeldt, M. Grätzel, W. Tress, *Nat. Energy* **2018**, *3*, 61.
[22] M. V. Khenkin, K. M. A., I. Visoly-Fisher, S. Kolusheva, Y. Galagan, F. Di Giacomo, O. Vukovic, B. R. Patil, G. Sherafatipour, V. Turkovic, H.-G. Rubahn, M. Madsen, A. V. Mazanik, E. A. Katz, *ACS Appl. Energy Mater.* **2018**, *1*, 799.
[23] W. Tress, M. Yavari, K. Domanski, P. Yadav, B. Niesen, J. P. Correa Baena, A. Hagfeldt, M. Graetzel, *Energy Environ. Sci.* **2018**, *11*, 151.
[24] M. V. Khenkin, K. M. Anoop, I. Visoly-Fisher, Y. Galagan, F. D. Giacomo, B. R. Patil, G. Sherafatipour, V. Turkovic, M. Madsen, T. Merckx, G. Uytterhoeven, J. P. A. Bastos, T. Aernouts, F. Brunetti, M. Lira-Cantu, E. A. Katz, *Energy Environ. Sci.* **2018**, *11*, 739.
[25] K. Domanski, B. Roose, T. Matsui, M. Saliba, S.-H. Turren-Cruz, J.-P. Correa-Baena, C. R. Carmona, G. Richardson, J. M. Foster, F. De Angelis, J. M. Ball, A. Petrozza, N. Mine, M. K. Nazeeruddin, W. Tress, M. Gratzel, U. Steiner, A. Hagfeldt, A. Abate, *Energy Environ. Sci.* **2017**, *10*, 604.
[26] W. Tress, K. Domanski, B. Carlsen, A. Agarwalla, E. A. Alharbi, M. Graetzel, A. Hagfeldt, *Nat. Energy* **2019**, *4*, 568.
[27] F. Huang, L. Jiang, A. R. Pascoe, Y. Yan, U. Bach, L. Spiccia, Y.-B. Cheng, *Nano Energy* **2016**, *27*, 509.
[28] W. Nie, J.-C. Blancon, A. J. Neukirch, K. Appavoo, H. Tsai, M. Chhowalla, M. A. Alam, M. Y. Sfeir, C. Katan, J. Even, S. Tretiak, J. J. Crochet, G. Gupta, A. D. Mohite, *Nat. Commun.* **2016**, *7*, 11574.
[29] B. P. Finkenauer, K. M. Akriti, L. Dou, *ACS Appl. Mater. Interfaces* **2022**, *14*, 24073.
[30] Z. Xiao, Y. Yuan, Y. Shao, Q. Wang, Q. Dong, C. Bi, P. Sharma, A. Gruverman, J. Huang, *Nat. Mater.* **2015**, *14*, 193.
[31] D. R. Ceratti, A. V. Cohen, R. Tenne, Y. Rakita, L. Snarski, N. P. Jasti, L. Cremonesi, R. Cohen, M. Weitman, I. Rosenhek-Goldian, I. Kaplan-Ashiri, T. Bendikov, V. Kalchenko, M. Elbaum, M. A. C. Potenza, L. Kronik, G. Hodes, D. Cahen, *Mater. Horiz.* **2021**, *8*, 1570.
[32] D. R. Ceratti, Y. Rakita, L. Cremonesi, R. Tenne, V. Kalchenko, M. Elbaum, D. Oron, M. A. C. Potenza, G. Hodes, D. Cahen, *Adv. Mater.* **2018**, *30*, 1706273.
[33] Y. Yu, F. Zhang, H. Yu, *Sol. Energy* **2020**, *209*, 408.
[34] C. Zhao, B. Chen, X. Qiao, L. Luan, K. Lu, B. Hu, *Adv. Energy Mater.* **2015**, *5*, 1500279.
[35] W. Song, T. Aernouts, *J. Phys.: Energy* **2020**, *2*, 021003.
[36] M. Babics, M. De Bastiani, E. Ugur, L. Xu, H. Bristow, F. Toniolo, W. Raja, A. S. Subbiah, J. Liu, L. V. Torres Merino, E. Aydin, S. Sarwade, T. G. Allen, A. Razzaq, N. Wehbe, M. F. Salvador, S. De Wolf, *Cell Reports Phys. Sci.* **2023**, *4*, 101280.
[37] M. Remec, Š. Tomšič, M. Khenkin, Q. Emery, J. Li, F. Scheler, B. Glažar, M. Jankovec, M. Jošt, E. Unger, S. Albrecht, R. Schlatmann, B. Lipovšek, C. Ulbrich, M. Topič, *Adv. Energy Mater.* **2024**, *14*, 2304452.
[38] N. Li, Y. Jia, Y. Guo, N. Zhao, *Adv. Mater.* **2022**, *34*, 2108102.
[39] F. Zhou, Y. Liu, X. Shen, M. Wang, F. Yuan, Y. Chai, *Adv. Funct. Mater.* **2018**, *28*, 1800080.
[40] Y. Zhang, Q. Song, G. Liu, Y. Chen, Z. Guo, N. Li, X. Niu, Z. Qiu, W. Zhou, Z. Huang, C. Zhu, H. Zai, S. Ma, Y. Bai, Q. Chen, W. Huang, Q. Zhao, H. Zhou, *Nat. Photonics* **2023**, *17*, 1066.
[41] M. Prete, M. V. Khenkin, D. Glowienka, B. R. Patil, J. S. Lissau, I. Dogan, J. L. Hansen, T. Leißner, J. Fiutowski, H. G. Rubahn, B. Julsgaard, P. Balling, V. Turkovic, Y. Galagan, E. A. Katz, M. Madsen, *ACS Appl. Energy Mater.* **2021**, *4*, 6562.
[42] T. Tayagaki, K. Yamamoto, T. N. Murakami, M. Yoshita, *Sol. Energy Mater. Sol. Cells* **2023**, *257*, 112387.
[43] L. T. Schelhas, Z. Li, J. A. Christians, A. Goyal, P. Kairys, S. P. Harvey, D. H. Kim, K. H. Stone, J. M. Luther, K. Zhu, V. Stevanovic, J. J. Berry, *Energy Environ. Sci.* **2019**, *12*, 1341.
[44] Y. Zhao, T. Heumueller, J. Zhang, J. Luo, O. Kasian, S. Langner, C. Kupfer, B. Liu, Y. Zhong, J. Elia, A. Osvet, J. Wu, C. Liu, Z. Wan, C. Jia, N. Li, J. Hauch, C. J. Brabec, *Nat. Energy* **2022**, *7*, 144.
[45] M. Koehl, M. Heck, S. Wiesmeier, J. Wirth, *Sol. Energy Mater. Sol. Cells* **2011**, *95*, 1638.
[46] X. Zhao, T. Liu, Q. C. Burlingame, T. Liu, R. Holley, G. Cheng, N. Yao, F. Gao, Y.-L. Loo, *Science* **2022**, *377*, 307.
[47] T. Tayagaki, H. Kobayashi, K. Yamamoto, T. N. Murakami, M. Yoshita, *Sol. Energy Mater. Sol. Cells* **2023**, *263*, 112583.
[48] J. Thiesbrummel, S. Shah, E. Gutierrez-Partida, F. Zu, F. Peña-Camargo, S. Zeiske, J. Diekmann, F. Ye, K. P. Peters, K. O. Brinkmann, P. Caprioglio, A. Dasgupta, S. Seo, F. A. Adeleye, J. Warby, Q. Jeangros, F. Lang, S. Zhang, S. Albrecht, T. Riedl, A. Armin, D. Neher, N. Koch, Y. Wu, V. M. Le Corre, H. Snaith, M. Stolterfoht, *Nat. Energy* **2024**, *9*, 664.
[49] A. These, L. J. A. Koster, C. J. Brabec, V. M. Le Corre, *Adv. Energy Mater.* **2024**, *14*, 2400055.
[50] S. Paek, S. B. Khan, M. Franckevičius, R. Gegevičius, O. A. Syzgantseva, M. A. Syzgantseva, S. Kinche, A. M. Asiri, C. Roldán-Carmona, M. K. Nazeeruddin, *J. Mater. Chem. A* **2021**, *9*, 5374.
[51] J. A. Christians, P. Schulz, J. S. Tinkham, T. H. Schloemer, S. P. Harvey, B. J. Tremolet de Villers, A. Sellinger, J. J. Berry, J. M. Luther, *Nat. Energy* **2018**, *3*, 68.
[52] Y. A. Olanrewaju, K. Orisekeh, O. V. Oyelade, R. K. Koech, R. Ichwani, A. I. Ebunu, D. I. Amune, A. Bello, V. C. Anye, O. K. Oyewole, W. O. Soboyejo, *Effects of temperature-dependent burn-in decay on the performance of triple cation mixed halide perovskite solar cells*, AIP Advances, Melville, NY **2022**, *12*.
[53] A. D. Sheikh, R. Munir, M. A. Haque, A. Bera, W. Hu, P. Shaikh, A. Amassian, T. Wu, *ACS Appl. Mater. Interfaces* **2017**, *9*, 35018.
[54] J. A. Schwenzer, L. Rakocevic, R. Gehlhaar, T. Abzieher, S. Gharibzadeh, S. Moghadamzadeh, A. Quintilla, B. S. Richards, U. Lemmer, U. W. Paetzold, *ACS Appl. Mater. Interfaces* **2018**, *10*, 16390.
[55] M. Chen, Y. Dong, Y. Zhang, X. Zheng, G. R. McAndrews, Z. Dai, Q. Jiang, S. You, T. Liu, S. P. Harvey, K. Zhu, V. Oliveto, A. Jackson, R. Witteck, L. M. Wheeler, N. P. Padture, P. J. Dyson, M. D. McGehee, M. K. Nazeeruddin, M. C. Beard, J. M. Luther, *ACS Energy Lett.* **2024**, *9*, 2582.
[56] Z. Zhang, H. Wang, T. J. Jacobsson, J. Luo, *Nat. Commun.* **2022**, *13*, 7639.
[57] C. C. Boyd, R. Cheacharoen, T. Leijtens, M. D. McGehee, *Chem. Rev.* **2019**, *119*, 3418.
[58] Q. C. Burlingame, Y.-L. Loo, E. A. Katz, *Nat. Energy* **2023**, *8*, 1300.
[59] M. Saliba, J.-P. Correa-Baena, C. M. Wolff, M. Stolterfoht, N. Phung, S. Albrecht, D. Neher, A. Abate, *Chem. Mater.* **2018**, *30*, 4193.
[60] L. Shi, M. P. Bucknall, T. L. Young, M. Zhang, L. Hu, J. Bing, D. S. Lee, J. Kim, T. Wu, N. Takamure, D. R. McKenzie, S. Huang, M. A. Green, A. W. Y. Ho-Baillie, *Science* **2020**, *368*, eaba2412.